

# Revisiting Min-Max Optimization Problem in Adversarial Training

Sina Hajer Ahmadi, Hassan Bahrami  
Electrical and Computer Engineering  
University of Waterloo  
Waterloo, Ontario

**Abstract**—The rise of computer vision applications in the real world puts the security of the deep neural networks at risk. Recent works demonstrate that convolutional neural networks are susceptible to adversarial examples - where the input images look similar to the natural images but are classified incorrectly by the model. To provide a rebuttal to this problem, we propose a new method to build robust deep neural networks against adversarial attacks by reformulating the saddle point optimization problem in [16]. Our proposed method offers significant resistance and a concrete security guarantee against multiple adversaries. The goal of this paper is to act as a stepping stone for a new variation of deep learning models which would lead towards fully robust deep learning models.

**Index Terms**—adversarial attacks, DNN, CNN, PGD, CW, minmax

## I. INTRODUCTION

Convolutional Neural Networks (CNNs) are recently gaining popularity in numerous [15] computer vision tasks. Some examples include face detection, self-driving or autonomous cars and malware detection. The wide use of CNNs makes it prone to adversarial attacks and developing security measures against becomes crucial. These attacks are imperceptible to the naked eye and subtly attack the image in a way that only changes the image slightly but which is enough to fool the model completely. To design adversarial attack resistant models is becoming a crucial design goal.

### A. Literature Review

Making the machine learning model more robust boils down to security [3] reasons to protect it against adversarial attacks. Adversarial robust models can be interpreted [18], [21] better and can be generalized better [4], [25]. Adversarial training deals with training the model on adversarial examples [9], [16]. Currently, machine learning practitioners favor adversarial training because (a) achieve higher robustness, (b) can be scaled to the state-of-the-art deep networks without affecting the inference time [7] and (c) can deal with different attacks. Adversarial training can be pictured as a robust optimization problem [16], [19] which takes the form of a non-convex non-concave min-max problem. However, computing the optimal adversarial examples is an NP-hard problem [2], [22]. In [16] adversarial training relies on approximation methods to solve the inner maximization problem. The PGD (projected gradient descent) attack [16] is successfully used where multiple steps

of projected gradient descent are performed. It is widely accepted that models trained using PGD attack [16] are robust since small adversarial trained networks can be formally verified [5], [20], [23], and larger models could not be broken on public challenges [12], [16], [24]. [8] evaluated the majority of recently published defenses and concluded that the standard  $l_\infty$  PGD training achieves the best empirical robustness; a result which can only be improved using semi-supervised approaches [1], [6], [13]. In contrast to that [8] claim that over improving the standard PGD training had overestimated the robustness of their model. From all these experiments it is evident that adversarial training is the key algorithm for robust deep learning and performing it efficiently is of paramount importance. [16] observed that adversarial trained models do not perform well on adversarial perturbed test data. It was observed that there is a stark contrast and a huge gap between the training accuracy and the test accuracy on the adversarial data. From these differences and gaps it can be inferred that the training is severely over-fitting the model.

In this paper, to tackle the above-mentioned problems, we reformulate the min-max optimization problem discussed in [16]. Unlike [16], our method does not exploit the gradient of loss function for the inner maximization problem. Yet, it solves the inner maximization problem from the probabilistic perspective. To be more specific, first, a prior distribution for the allowed perturbation, namely  $\delta$ , is considered. Afterward, by sampling from this distribution, for each sample a sufficiently large number of attacked versions, say  $k$ , is generated. Moreover, the cross-entropy loss function, namely  $L(\cdot)$ , is replaced by  $e^{\lambda L(\cdot)}$  for some large value of  $\lambda$ . As proven later, this will guarantee that the sum of loss function values for all of the  $k$  attacked samples is proportional to the maximum loss value for that sample. This will resolve the problem of getting stuck in the local maximum obtained by PGD algorithm.

We should also mention that the same idea has been deployed to train a fair federated learning model where the authors try to solve a multi objective optimization problem [11], [14], [17].

### B. Organization

The organization of the paper is as follows. In section II, we first briefly elaborate how [16] have performed adversarial training and then propose our own method that reformulates the saddle point optimization problem. In section III we

describe 3 different distributions to sample the perturbations from. Section IV summarizes the performance of our various models and compares them with the performance of the models in [16]. We conclude the paper in Section V by making concrete comments over the results of our approach and talk briefly about our future work.

## II. METHODOLOGY

### A. MadryLab Adversarial Training

In [16], the authors formulated the adversarial training as the following saddle point optimization problem

$$\arg \min_{\theta} \mathbb{E}_{(x,y) \sim \mathcal{D}} \{ \max_{\delta \in \mathcal{S}} L(\theta, x + \delta, y) \}, \quad (1)$$

where  $\mathcal{S}$  is the allowed set of perturbation. Then, they performed various experiments focusing on two key elements: a) train a sufficiently high capacity network, b) use the strongest possible adversary in training. In order to solve the inner maximization problem, they exploit projected gradient descent (PGD) starting from a random perturbation around the natural example. This algorithm effectively maximizes the loss of an example using only first order information. This approach demonstrated a steady decrease of training loss in the adversarial examples. They evaluated this trained model against a range of adversaries.

### B. Proposed Method

In our proposed method, we reformulate the saddle point optimization problem in [16].

**Assumptions:** we assume that loss function is smooth w.r.t. its inputs, and therefore w.r.t.  $\delta$ .

**Notations:**  $B_r(a)$  is an  $n$ -dimensional ball with radius  $r$  centered at  $a$ . Denote by  $\nabla L_x(\cdot)$  and  $\mathbf{H}_x$ , the gradient vector and Hermitian matrix of loss function w.r.t.  $x$ , respectively.

**Theorem 1.** For a large value of  $\lambda$ , the two following saddle point optimization problems are equivalent:

$$\arg \min_{\theta} \mathbb{E}_{(x,y) \sim \mathcal{D}} \{ \max_{\delta \in \mathcal{S}} L(\theta, x + \delta, y) \} \quad (2)$$

$$\arg \min_{\theta} \mathbb{E}_{(x,y) \sim \mathcal{D}} \left\{ \int_{\delta \in \mathcal{S}} e^{\lambda L(\theta, x + \delta, y)} d\delta \right\} \quad (3)$$

*Proof.* To prove Theorem 1, it is sufficient to show that:

$$\max_{\delta \in \mathcal{S}} L(\theta, x + \delta, y) = \kappa \times \int_{\delta \in \mathcal{S}} e^{\lambda L(\theta, x + \delta, y)} d\delta, \quad (4)$$

where  $\kappa$  is a constant number. To this end, assume that  $\delta^*$  yields the maximum value in 4. Based on where the loss function attains its maximum value on  $\mathcal{S}$ , we consider the following cases (for notational simplicity, we denote  $L(\theta, x + \delta, y)$  by  $L(\delta)$ ):

1) If there is a unique interior point  $\delta^* \in \mathcal{S}$  attaining the maximum value. Since the loss function is smooth w.r.t.  $\delta$ , then  $\nabla L(\delta^*) = 0$ . We prove that for large  $\lambda$ ,

$$\frac{\int_{\delta \in \mathcal{S}} e^{\lambda L(\delta)} d\delta}{e^{\lambda L(\delta^*)} \sqrt{\frac{(2\pi)^n}{\lambda \det(-\mathbf{H}_{\delta^*})}}} \rightarrow 1, \quad (5)$$

or equivalently, we prove that

$$1 \leq \frac{\int_{\delta \in \mathcal{S}} e^{\lambda L(\delta)} d\delta}{e^{\lambda L(\delta^*)} \sqrt{\frac{(2\pi)^n}{\lambda \det(-\mathbf{H}_{\delta^*})}}} \leq 1, \quad (6)$$

for some large  $\lambda$ . To this aim, we first establish upper and lower bounds for the loss function in the small vicinity around  $\delta^*$ . Based on the Taylor theorem, in the small ball  $B_r(\delta^*)$  the loss function  $L(\delta)$  is bounded by:

$$\begin{aligned} L(\delta^*) + \frac{1}{2}(\delta - \delta^*)^T \mathbf{H}_{\delta^*} (\delta - \delta^*) - \mathcal{R}_2(\delta) &< L(\delta) \\ &< L(\delta^*) + \frac{1}{2}(\delta - \delta^*)^T \mathbf{H}_{\delta^*} (\delta - \delta^*) + \mathcal{R}_2(\delta), \end{aligned} \quad (7)$$

where  $\mathcal{R}_2(\delta)$  is the second remainder of Taylor expansion. By defining

$$\epsilon = \frac{\mathcal{R}_2(\delta)}{\max_{\delta \in B_r(\delta^*)} (\delta - \delta^*)^T (\delta - \delta^*)}, \quad (8)$$

inequalities in 7 are simplified to

$$\begin{aligned} L(\delta^*) + \frac{1}{2}(\delta - \delta^*)^T (\mathbf{H}_{\delta^*} - \epsilon) (\delta - \delta^*) &< L(\delta) \\ &< L(\delta^*) + \frac{1}{2}(\delta - \delta^*)^T (\mathbf{H}_{\delta^*} + \epsilon) (\delta - \delta^*), \end{aligned} \quad (9)$$

and therefore

$$\begin{aligned} e^{\lambda(L(\delta^*) + \frac{1}{2}(\delta - \delta^*)^T (\mathbf{H}_{\delta^*} - \epsilon) (\delta - \delta^*))} &< e^{\lambda L(\delta)} \\ &< e^{\lambda(L(\delta^*) + \frac{1}{2}(\delta - \delta^*)^T (\mathbf{H}_{\delta^*} + \epsilon) (\delta - \delta^*))}. \end{aligned} \quad (10)$$

*Lower Bound:* From the first inequality 10

$$\begin{aligned} &\int_{\delta \in \mathcal{S}} e^{\lambda L(\delta)} d\delta \\ &= \int_{\delta \in B_r(\delta^*)} e^{\lambda L(\delta)} d\delta + \int_{\delta \in \mathcal{S} \setminus B_r(\delta^*)} e^{\lambda L(\delta)} d\delta \end{aligned} \quad (11)$$

$$\geq \int_{\delta \in B_r(\delta^*)} e^{\lambda L(\delta)} d\delta \quad (12)$$

$$\geq \int_{\delta \in B_r(\delta^*)} e^{\lambda(L(\delta^*) + \frac{1}{2}(\delta - \delta^*)^T (\mathbf{H}_{\delta^*} - \epsilon) (\delta - \delta^*))} d\delta \quad (13)$$

$$= e^{\lambda L(\delta^*)} \int_{\delta \in B_r(\delta^*)} e^{\frac{\lambda}{2}(\delta - \delta^*)^T (\mathbf{H}_{\delta^*} - \epsilon) (\delta - \delta^*)} d\delta \quad (14)$$

$$= \frac{e^{\lambda L(\delta^*)}}{\sqrt{\lambda}} \int_{\delta \in B_{r\sqrt{\lambda}}(0)} e^{\frac{-1}{2}y^T (-\mathbf{H}_{\delta^*} + \epsilon)y} dy, \quad (15)$$

where (15) is obtained by setting  $y = \sqrt{\lambda}(\delta - \delta^*)$ . Note that since  $L(\theta)$  is smooth and attained its maximum value in  $\mathcal{S}$ ,  $\mathbf{H}_{\delta^*}$  is negative definite in small vicinity around  $\delta^*$ , and therefore  $-\mathbf{H}_{\delta^*}$  is positive definite. Thus,  $-\mathbf{H}_{\delta^*} + \epsilon$  is also positive definite (maybe in smaller ball, I will make this more accurate). Hence, if  $\lambda$  is large enough, by using multivariate normal integral, (15) is simplified to  $\sqrt{\frac{(2\pi)^n}{\det(-\mathbf{H}_{\delta^*} + \epsilon)}}$  (note that as  $(-\mathbf{H}_{\delta^*} + \epsilon)$  is positive definite, its determinant is always positive). Hence,

$$\int_{\delta \in \mathcal{S}} e^{\lambda L(\delta)} d\delta \geq e^{\lambda L(\delta^*)} \sqrt{\frac{(2\pi)^n}{\lambda \det(-\mathbf{H}_{\delta^*} + \epsilon)}} \quad (16)$$

*Upper Bound:* Since  $\delta^* \in B_r(\delta^*)$ , for  $\delta \in \mathcal{S} \setminus B_r(\delta^*)$ ,  $L(\theta) < L(\delta^*) - \eta$  for some  $\eta > 0$ . Therefore,

$$\int_{\delta \in \mathcal{S} \setminus B_r(\delta^*)} e^{\lambda(L(\delta))} d\delta \leq \mathbf{Vol}(\mathcal{S} \setminus B_r(\delta^*)) \left( e^{\lambda(L(\delta^*) - \eta)} \right), \quad (17)$$

where  $\mathbf{Vol}(\cdot)$  denote the volume. Therefore, by using the second inequality in (10), and equations (11) and (17)

$$\begin{aligned} & \int_{\delta \in \mathcal{S}} e^{\lambda(L(\delta))} d\delta \\ & \leq \int_{\delta \in B_r(\delta^*)} e^{\lambda(L(\delta^*) + \frac{1}{2}(\delta - \delta^*)^T (\mathbf{H}_{\delta^*} + \epsilon)(\delta - \delta^*))} d\delta \\ & + \mathbf{Vol}(\mathcal{S} \setminus B_r(\delta^*)) \left( e^{\lambda(L(\delta^*) - \eta)} \right) \end{aligned} \quad (18)$$

$$\begin{aligned} & = \frac{e^{\lambda(L(\delta^*))}}{\sqrt{\lambda}} \int_{\delta \in B_{r\sqrt{\lambda}}(0)} e^{\frac{-1}{2}y^T(-\mathbf{H}_{\delta^*} - \epsilon)y} dy \\ & + \mathbf{Vol}(\mathcal{S} \setminus B_r(\delta^*)) \left( e^{\lambda(L(\delta^*) - \eta)} \right) \end{aligned} \quad (19)$$

$$= e^{\lambda L(\delta^*)} \sqrt{\frac{(2\pi)^n}{\lambda(\det(-\mathbf{H}_{\delta^*} - \epsilon))}} + \mathbf{Vol}(\mathcal{S} \setminus B_r(\delta^*)) \left( e^{\lambda(L(\delta^*) - \eta)} \right). \quad (20)$$

If we divide both sides of the above inequality by

$$e^{\lambda L(\delta^*)} \sqrt{\frac{(2\pi)^n}{\lambda(\det(-\mathbf{H}_{\delta^*}))}}, \quad (21)$$

and then considering  $\lambda$  is a large number, we obtain

$$\begin{aligned} & \frac{\int_{\delta \in \mathcal{S}} e^{\lambda L(\delta)} d\delta}{e^{\lambda L(\delta^*)} \sqrt{\frac{(2\pi)^n}{\lambda \det(-\mathbf{H}_{\delta^*})}}} \\ & \leq \mathbf{Vol}(\mathcal{S} \setminus B_r(\delta^*)) (e^{-\lambda \eta}) \sqrt{\frac{\lambda \det(-\mathbf{H}_{\delta^*})}{(2\pi)^n}} \\ & + \sqrt{\frac{\det(-\mathbf{H}_{\delta^*})}{\det(-\mathbf{H}_{\delta^*} - \epsilon)}} = \sqrt{\frac{\det(-\mathbf{H}_{\delta^*})}{\det(-\mathbf{H}_{\delta^*} - \epsilon)}}, \end{aligned} \quad (22)$$

which completes the proof for case 1.

2) If the maximum accrues at the edge of  $\mathcal{S}$ , then  $\nabla L(\delta^*) \neq 0$ . Then using the first order Taylor approximation we have

$$L(\theta) \approx L(\theta^*) + \nabla L(\theta^*)^T (\theta - \theta^*). \quad (23)$$

Using the same method used for case 1, it could be proven that

$$\frac{\int_{\delta \in \mathcal{S}} e^{\lambda L(\delta)} d\delta}{\frac{e^{\lambda L(\delta^*)}}{\lambda(\nabla L(\theta^*))^n}} \rightarrow 1. \quad (24)$$

3) If there are  $k$  absolute maximum occurring at multiple points, then [10]

$$\int_{\delta \in \mathcal{S}} e^{\lambda L(\delta)} d\delta = \left( \sum_{i=1}^k \kappa_i \right) e^{\lambda L(\theta^*)}. \quad (25)$$

□

### III. SAMPLING METHODS

To evaluate the integral in (3), we assume a prior distribution for  $\delta \in \mathcal{S}$ . In the following, we consider three different prior distributions.

#### A. Uniform Sampling

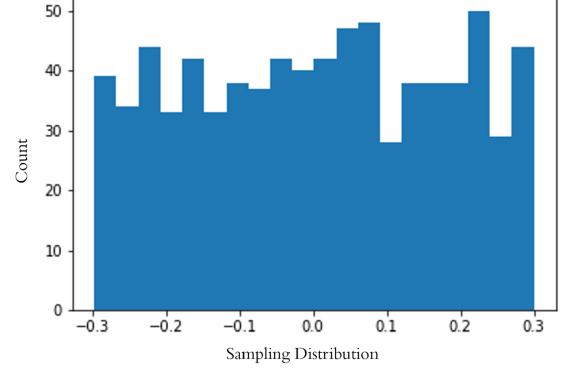


Fig. 1. Uniform Distribution Sampling

The first set of experiments that we carried out was sample the perturbations uniformly  $-\epsilon$  to  $+\epsilon$ . We realised that the perturbations produced in this approach are fairly different than the perturbations produced when the network is attacked with different attacks like PGD and CW (Carlini and Wager). We further tried to model the perturbations based on these attacks.

#### B. Sampling Based on PGD and CW

In the next approach, we model the perturbations based on the PGD attack. To achieve this we used this formula:

$$\text{Perturbations} = X_{\text{Attacked}} - X_{\text{original}} \quad (26)$$

The distribution of the perturbations on a batch size of 50 images look like this: Most of the values are concentrated

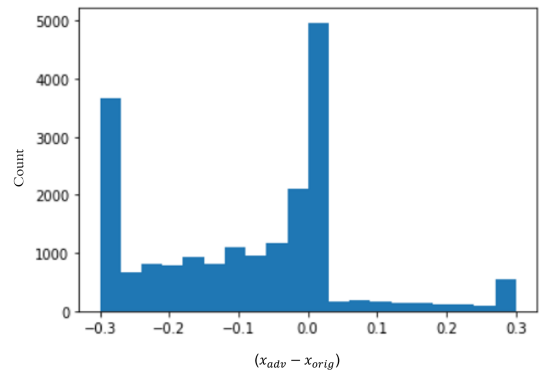


Fig. 2. Sampling based on PGD Perturbations

between  $-0.3$  and  $0$  and the values have a spike for  $-0.3$  and  $0$ . In our approach we sampled over these values and added these values to the image for training.

□

We also modeled the distribution for the CW attack but ended up using the PGD attack distribution in our implementation.

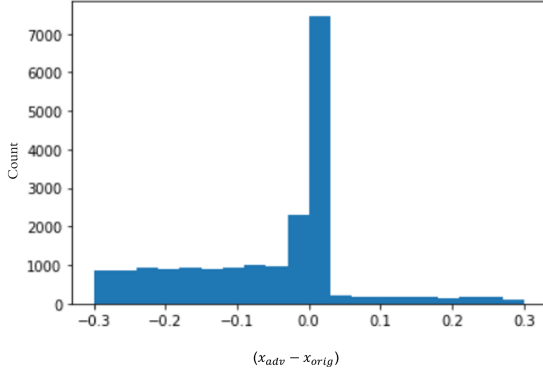


Fig. 3. Sampling based on CW Perturbations

We observed that there is a uniform distribution from  $-0.3$  to  $0$  and most of the values are concentrated at  $0$ .

### C. DCT Domain Sampling

We also carried out two experiments in the DCT domain. The general idea of carrying out our experiments in the DCT domain is that instead of sampling the perturbation and adding them in the pixel domain, we sampled the perturbation and added them in the DCT domain. This was the process carried out by us:

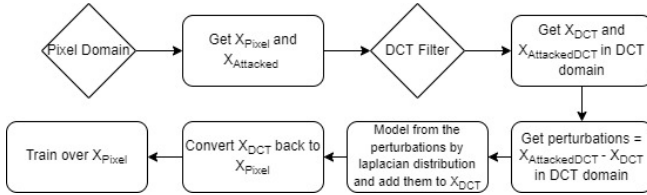


Fig. 4. The diagram for simulating the perturbation in the DCT domain.

#### 1) Sampling from Laplacian Distribution:

- We got  $X_{Pixel}$  (Original Image) and  $X_{Attacked}$  Images from the original Image.
- We passed them through a DCT filter and got their respective in the DCT domain ( $X_{DCT}$  and  $X_{AttackedDCT}$ ).
- We then subtracted them to get the perturbations ( $X_{AttackedDCT} - X_{DCT}$ ) in the DCT domain.
- We then modeled these perturbations using the Laplacian distribution (see Fig. 5).
- We sampled from these perturbations and added them to  $X_{DCT}$ .
- Converted  $X_{DCT}$  from the DCT domain back the  $X_{Pixel}$  in the pixel domain.
- Trained the network over  $X_{Pixel}$ .

#### 2) Sampling from Empirical Probability Density Function:

The basic idea for this approach is very similar to the previous approach. In the previous approach we model the perturbations using the Laplacian distribution and then sample them these

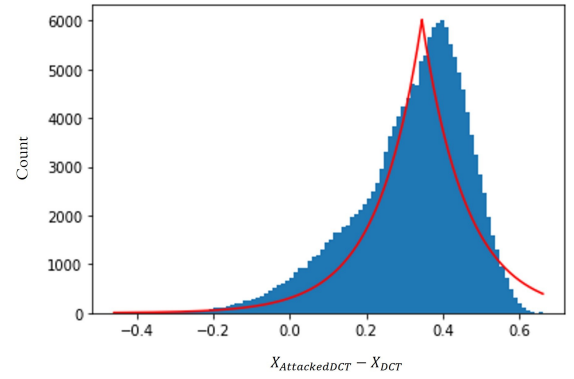


Fig. 5. The red line is the Laplacian distribution graph and the blue histogram is the empirical pdf of perturbation in DCT domain.

values in DCT domain. But in this approach we directly sample from the perturbations got in the DCT domain and add them to the image in the DCT domain. We then convert this image back to the pixel domain and train over these images. So the basic idea for this method is similar to the last one except the way of sampling is different.

## IV. EXPERIMENTS AND RESULTS

To justify the effectiveness of the proposed method, some experiments are carried out over the MNIST dataset.

Based on the experiments we performed, the highest robustness achieved in our method is when we sample from the empirical pdf in either spacial or DCT domain. Hence, we only report the results for this type of sampling and compare the results with those reported in [16]. The number of samples used for our simulations is 100, so the batch size is 100 times that of the original one. In the following, first, we try different values for the exponential component  $\lambda$  in the Spacial and the DCT domain for  $\epsilon = \{0.1, 0.2, 0.3\}$ , and compare the accuracy of our models with that of the [16]. Afterward, we compare the robustness of our model trained with images in the Spatial domain, with exponential component  $\lambda = 1$  and strength of the attack  $\epsilon = 0.3$  with the [16] model trained with  $\epsilon = 0.3$ .

### A. Performance Analysis against PGD attack

In this subsection we analyze the accuracy of our models trained a over  $\epsilon = 0.1, 0.2$  and  $0.3$ .

#### 1) $\epsilon = 0.1$

We analyze the performance of our model trained on  $\epsilon = 0.1$  and with exponential components  $\lambda = 1, 2$  and compare it with the accuracy of the MadryLab model trained on  $\epsilon = 0.1$ . See Figure 6 and Table 1.

TABLE I  
ACCURACY RESULTS FOR  $\epsilon = 0.1$

PGD	$\lambda = 1$	$\lambda = 2$	Madry Acc
MadryLab Model	-	-	95.34%
Spatial Domain	98.24%	98.24%	-
DCT Domain	96.76%	90.28%	-

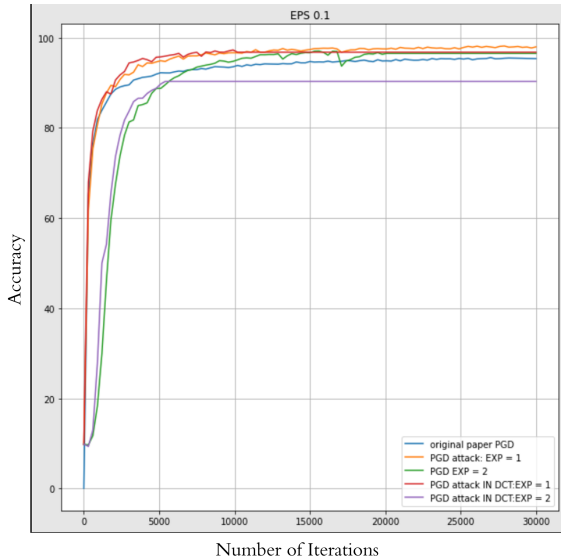


Fig. 6. Performance of our adversarial trained models for exponential component  $\lambda = 1, 2$  in the Spatial and DCT domain compared with the MadryLab adversarial trained model for  $\epsilon = 0.1$ .

The observations noted for  $\epsilon = 0.1$  are that three of our trained models outperform the MadryLab trained model. For the exponential component  $\lambda = 1$ , we outperform MadryLab with an accuracy of 98.24% in the Spatial Domain and 96.76% in the DCT Domain. For the exponential component  $\lambda = 2$ , we outperform the MadryLab only in the Spatial Domain with an accuracy of 96.5%. The accuracy noted for the MadryLab model for  $\epsilon = 0.1$  is 95.34%.

The general trend of all the models seems similar and achieves a higher accuracy in the initial iterations and maintain that as the number of iterations increase.

2)  $\epsilon = 0.2$

We analyze the performance of our models trained on  $\epsilon = 0.2$  and with exponential components  $\lambda = 1, 2, 3, 4$  and compare it with the accuracy of the MadryLab model trained on  $\epsilon = 0.2$ . See Figure 7 and Table 2.

TABLE II  
ACCURACY RESULTS FOR  $\epsilon = 0.2$

PGD	$\lambda = 1$	$\lambda = 2$	$\lambda = 3$	$\lambda = 4$	Madry Acc
MadryLab Model	-	-	-	-	89.17%
Spatial Domain	95.06%	93.64%	81.38 %	86.95%	-
DCT Domain	94.18%	-	-	-	-

For  $\epsilon = 0.2$ , three of our trained models heavily outperform the Madrylab model. In the Spatial Domain, for the exponential component  $\lambda = 1, 2$ , we achieved an accuracy of 95.06% and 93.64% respectively. In the DCT domain, for the exponential component  $\lambda = 1$ , we achieved an accuracy of 94.18%. Whereas the accuracy noted for the MadryLab model for  $\epsilon = 0.2$  is 89.17%.

The general trend of the curves is similar to the trend of the curves for  $\epsilon = 0.1$  except for when the exponential

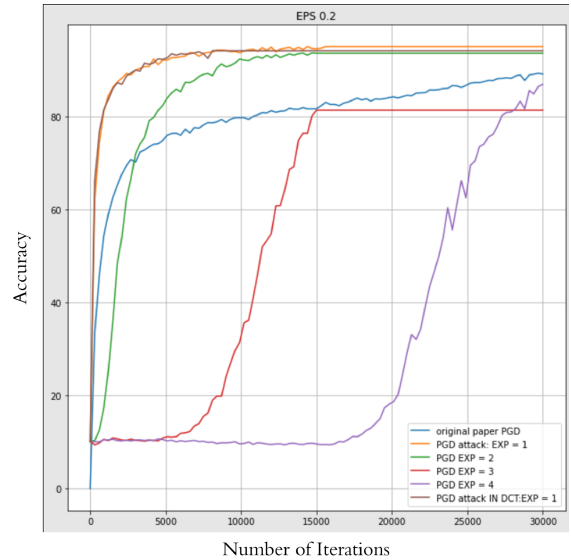


Fig. 7. Performance of our adversarial trained models for exponential component  $\lambda = 1, 2, 3, 4$  in the Spatial and for exponential component  $\lambda = 1$  in the DCT domain compared with the MadryLab adversarial trained model for  $\epsilon = 0.2$ .

component  $\lambda$  was set at a higher value. It is noteworthy that when the exponential component  $\lambda$  is higher ( $\lambda = 2, 3$ ) the accuracy is initially low but picks up exponentially. The accuracy curve for higher values of  $\lambda$  follows a similar trend for the exponential graph of its value.

3)  $\epsilon = 0.3$

We analyze the performance of our models trained on  $\epsilon = 0.3$  and with exponential components  $\lambda = 1, 2, 3, 4$  and compare it with the accuracy of the MadryLab model trained on  $\epsilon = 0.3$ . See Figure 7 and Table 2.

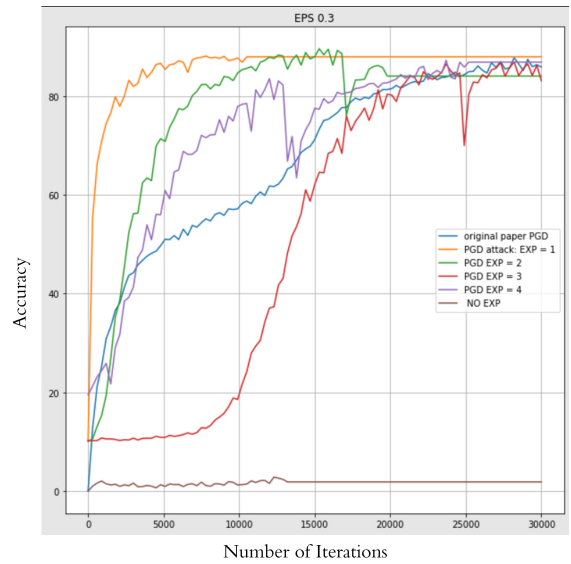


Fig. 8. Performance of our adversarial trained models for exponential component  $\lambda = 1, 2, 3, 4$  in the Spatial compared with the MadryLab adversarial trained model for  $\epsilon = 0.3$ .

TABLE III  
ACCURACY RESULTS FOR  $\epsilon = 0.3$

PGD	$\lambda = 1$	$\lambda = 2$	$\lambda = 3$	$\lambda = 4$	Madry Acc
MadryLab Model	-	-	-	-	85.86%
Spatial Domain	87.92%	88.8%	83.89 %	87.22%	-

For  $\epsilon = 0.3$ , three of our trained models outperform the Madrylab model. In the Spatial Domain, for the exponential component  $\lambda = 1, 2$  and  $4$  we achieved an accuracy of 87.92%, 88.8% and 87.22% respectively. Whereas the accuracy noted for the MadryLab model for  $\epsilon = 0.3$  is 85.86%.

The trend for  $\epsilon = 0.3$  for all models is quite erratic and for higher values of the model converges much slower and the graph is similar to the exponential graph of its exponential component  $\lambda$ .

### B. Robustness Check against PGD adversaries of different strength

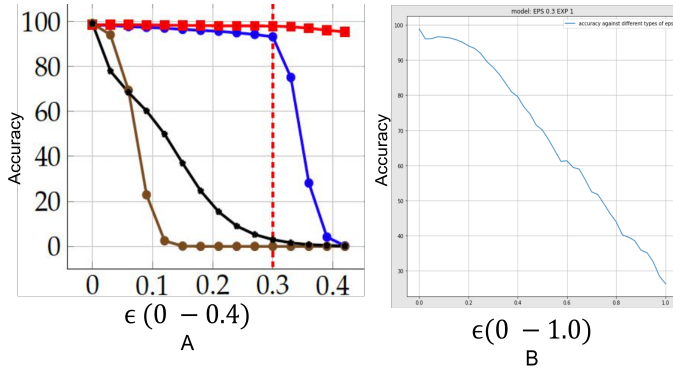


Fig. 9. A: Performance of Madrylab network against PGD adversaries of different strength (blue line). B: Performance of our adversarial trained network against PGD adversaries of different strength. The model was trained against  $\epsilon = 0.3$ .

In this subsection we test the robustness of our model by testing it over a range of  $\epsilon$  from 0 to 1. The model that we use is trained on  $\epsilon = 0.3$  and exponential component  $\lambda = 1$  and the training images are attacked in the Spatial Domain. We compare the robustness of our model with that of the MadryLab model.

In Figure 4a, for the Madrylab model, we observe that for  $\epsilon$  less or equal to the value used during training, the performance is equal if not better. But when  $\epsilon$  crosses its value for training, the accuracy plummets immediately and sinks to 0%. Whereas, in Figure 4b, for our model, the accuracy gradually decreases for higher values of  $\epsilon$ . So, compared with the Madrylab model, our model is more robust and dependent against stronger attacks.

## V. CONCLUSION

Our results suggest that deep neural network can be made resistant against adversarial attacks. Our theory of training the

images over PGD sampled perturbations and augmenting the data and batch size is reliable. Making the loss exponential aids our cause. We have proved that training the images by sampling them in both, spatial domain and DCT domain yields a high accuracy. Our different models both, in the spatial and DCT domain yield a higher accuracy that the model proposed by Madrylab. From the results, our adversarial models are more robust for stronger attacks than compared with the Madrylab model.

Our model is very robust for the MNIST dataset and achieves a high accuracy against the PGD attack for a wide range of  $\epsilon$  but does not do well against the CW attack. Our results show that, the methods that we have used lead to a significant increase in the robustness of the network. Our future work relies heavily on training and testing of the CIFAR10 dataset and testing our models on the FGSM attack.

## REFERENCES

- [1] Jean-Baptiste Alayrac, Jonathan Uesato, Po-Sen Huang, Alhussein Fawzi, Robert Stanforth, and Pushmeet Kohli. Are labels required for improving adversarial robustness? *Advances in Neural Information Processing Systems*, 32, 2019.
- [2] Maksym Andriushchenko and Nicolas Flammarion. Understanding and improving fast adversarial training. *Advances in Neural Information Processing Systems*, 33:16048–16059, 2020.
- [3] Battista Biggio and Fabio Roli. Wild patterns: Ten years after the rise of adversarial machine learning. *Pattern Recognition*, 84:317–331, 2018.
- [4] Alexey Bochkovskiy, Chien-Yao Wang, and Hong-Yuan Mark Liao. Yolov4: Optimal speed and accuracy of object detection. *arXiv preprint arXiv:2004.10934*, 2020.
- [5] Nicholas Carlini, Guy Katz, Clark Barrett, and David L Dill. Provably minimally-distorted adversarial examples. *arXiv preprint arXiv:1709.10207*, 2017.
- [6] Yair Carmon, Aditi Raghunathan, Ludwig Schmidt, John C Duchi, and Percy S Liang. Unlabeled data improves adversarial robustness. *Advances in Neural Information Processing Systems*, 32, 2019.
- [7] Jeremy Cohen, Elan Rosenfeld, and Zico Kolter. Certified adversarial robustness via randomized smoothing. In *International Conference on Machine Learning*, pages 1310–1320. PMLR, 2019.
- [8] Francesco Croce and Matthias Hein. Reliable evaluation of adversarial robustness with an ensemble of diverse parameter-free attacks. In *International conference on machine learning*, pages 2206–2216. PMLR, 2020.
- [9] Ian J Goodfellow, Jonathon Shlens, and Christian Szegedy. Explaining and harnessing adversarial examples. *arXiv preprint arXiv:1412.6572*, 2014.
- [10] Shayan Mohajer Hamidi. Training neural networks on remote edge devices for unseen class classification. *IEEE Signal Processing Letters*, 31:1004–1008, 2024.
- [11] Shayan Mohajer Hamidi and EN-HUI YANG. Adafed: Fair federated learning via adaptive common descent direction. *Transactions on Machine Learning Research*, 2024.
- [12] Shayan Mohajer Hamidi and Linfeng Ye. Robustness against adversarial attacks via learning confined adversarial polytopes. In *ICASSP 2024 - 2024 IEEE International Conference on Acoustics, Speech and Signal Processing (ICASSP)*, pages 5670–5674, 2024.
- [13] Dan Hendrycks, Kimin Lee, and Mantas Mazeika. Using pre-training can improve model robustness and uncertainty. In *International Conference on Machine Learning*, pages 2712–2721. PMLR, 2019.
- [14] Zeou Hu, Kiarash Shaloudegi, Guojun Zhang, and Yaoliang Yu. Fedmgda+: Federated learning meets multi-objective optimization. *arXiv preprint arXiv:2006.11489*, 2020.
- [15] Ajitesh Kumar. Real-world applications of convolutional neural network (cnn). <https://vitalflux.com/real-world-applications-of-convolutional-neural-networks/>, November 2021.
- [16] Aleksander Madry, Aleksandar Makelov, Ludwig Schmidt, Dimitris Tsipras, and Adrian Vladu. Towards deep learning models resistant to adversarial attacks. *arXiv preprint arXiv:1706.06083*, 2017.

- [17] Shayan Mohajer Hamidi and Oussama Damen. Fair wireless federated learning through the identification of a common descent direction. *IEEE Communications Letters*, 28(3):567–571, 2024.
- [18] Shibani Santurkar, Andrew Ilyas, Dimitris Tsipras, Logan Engstrom, Brandon Tran, and Aleksander Madry. Image synthesis with a single (robust) classifier. *Advances in Neural Information Processing Systems*, 32, 2019.
- [19] Uri Shaham, Yutaro Yamada, and Sahand Negahban. Understanding adversarial training: Increasing local stability of supervised models through robust optimization. *Neurocomputing*, 307:195–204, 2018.
- [20] Vincent Tjeng, Kai Xiao, and Russ Tedrake. Evaluating robustness of neural networks with mixed integer programming. *arXiv preprint arXiv:1711.07356*, 2017.
- [21] Dimitris Tsipras, Shibani Santurkar, Logan Engstrom, Alexander Turner, and Aleksander Madry. Robustness may be at odds with accuracy. *arXiv preprint arXiv:1805.12152*, 2018.
- [22] Lily Weng, Huan Zhang, Hongge Chen, Zhao Song, Cho-Jui Hsieh, Luca Daniel, Duane Boning, and Inderjit Dhillon. Towards fast computation of certified robustness for relu networks. In *International Conference on Machine Learning*, pages 5276–5285. PMLR, 2018.
- [23] Eric Wong, Leslie Rice, and J Zico Kolter. Fast is better than free: Revisiting adversarial training. *arXiv preprint arXiv:2001.03994*, 2020.
- [24] Hongyang Zhang, Yaodong Yu, Jiantao Jiao, Eric Xing, Laurent El Ghaoui, and Michael Jordan. Theoretically principled trade-off between robustness and accuracy. In *International conference on machine learning*, pages 7472–7482. PMLR, 2019.
- [25] Chen Zhu, Yu Cheng, Zhe Gan, Siqi Sun, Tom Goldstein, and Jingjing Liu. FreeLB: Enhanced adversarial training for natural language understanding. *arXiv preprint arXiv:1909.11764*, 2019.